Investigation of the cleaved surface of a $p-i-n$ laser using Kelvin probe force microscopy and two-dimensional physical simulations

F. Robin,[a] H. Jacobs,[b,c] O. Homan, A. Stemmer,[b] and W. Bächtold
Laboratory for Electromagnetic Fields and Microwave Electronics, ETH Center/ETZ, CH-8092 Zurich, Switzerland

(Received 2 August 1999; accepted for publication 17 March 2000)

We have investigated the cross-sectional electric field and potential distribution of a cleaved n^+-InP/InGaAsP/p^+-InP $p-i-n$ laser diode using Kelvin probe force microscopy (KFM) with a lateral resolution reaching 50 nm. The powerful characterization capabilities of KFM were compared with two-dimensional (2D) physics-based simulations. The agreement between simulations and KFM measurements regarding the main features of the electric field and potential is very good. However, the KFM yields a voltage drop between n- and p-doped InP regions which is 0.4 times the one simulated. This discrepancy is explained in terms of surface traps due to the exposure of the sample to the air and in terms of incomplete ionization. This hypothesis is confirmed by the 2D simulations. © *2000 American Institute of Physics.* [S0003-6951(00)00620-3]

In the past few years, the swift development of two-dimensional potential profile measurement techniques with high spatial resolution has paralleled the reduced dimensions of semiconductor devices to submicrometer scales. Much work has been done to develop Kelvin probe force microscopy,[1–3] a variation of the well-established atomic-force microscopy allowing a direct measurement of the local potential and electric field distributions based on the capacitance between a vibrating tip and the sample. Several contributions[4,5] have matured the Kelvin probe force microscopy (KFM) technique and Mizutani *et al.*[6] have measured the cross-sectional potential distribution of GaAs high electron mobility transistors under bias. Chavez-Pirson *et al.*[7] have studied the potential distribution of a cleaved GaAs/AlGaAs $n-i-p-i$ structure with a solution in the 50 nm range. Moreover, the above mentioned shrinkage of semiconductor devices dimensions as well as more powerful computing capabilities have encouraged the development of two-dimensional (2D) physics-based simulation tools.[8] These tools are based on models describing with great accuracy the internal physics of the devices, such as carrier statistics, transport phenomena, and thermal effects. However, only recent interest has been shown in simulating InP-based devices, mainly due to the lack of knowledge of the InP material system.[9] In this letter, we report the first cross-sectional investigation of n^+-InP/InGaAsP/p^+-InP $p-i-n$ laser diodes using KFM and 2D simulations. We first present the KFM studies of the laser diode. Then the 2D simulations are discussed, and finally the two techniques are compared.

The microscope used for the KFM measurements is based on a modified commercial atomic force microscopy (AFM) (Digital Instruments, Inc). Details of the experimental setup can be found elsewere.[10–12] Topography and surface potential are measured sequentially using the lift-mode technique to minimize cross-talk[10] (Fig. 1). The surface topography is acquired using TappingMode™. In KFM the tip geometry defines a transfer function which combines the detected KFM potential maps with the actual surface potential distribution.[12] For a given tip geometry we routinely calculate this transfer function by solving the three-dimensional electrostatic field distribution around the tip.[5] For the tips used in our experiments [Fig. 2(b)] the transfer function illustrated in Fig. 2(c) has been determined and has been experimentally confirmed.[5]

The $p-i-n$ laser diode studied in this work was grown by metal-organic chemical vapor deposition. The laser structure consists of an n-doped InP substrate ($N_D \approx 2\times10^{18}\,\mathrm{cm}^{-3}$), an n-doped InP layer ($N_D \approx 2\times10^{18}\,\mathrm{cm}^{-3}$), a nonintentionally doped 300-nm-thick InGaAsP active layer followed by a p-doped 1.7-μm-thick InP layer ($N_A \approx 1\times10^{18}\,\mathrm{cm}^{-3}$). A 180-nm-thick heavily doped InGaAs cap layer was grown last for good ohmic contacts. Additionally, a grading was grown between the InGaAsP and p-InP layers. Figure 2(a) shows an AFM topog-

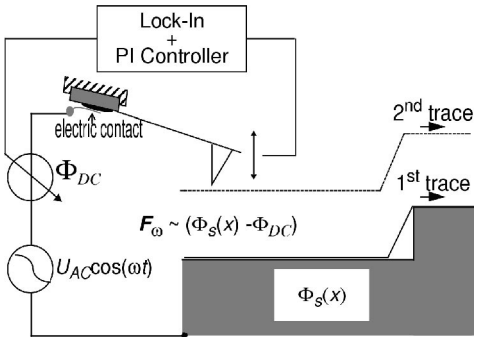

FIG. 1. Principle of KFM to detect the local surface potential distribution $\Phi_s(x)$. The feedback controller changes Φ_{dc} until F_ω becomes zero. Surface potential maps are obtained by recording the controlled dc tip potential Φ_{dc}. During the first scan line the surface topography is acquired using tapping mode. This topography is then retraced at a preset lift height (typically <20 nm) to detect the KFM potential using the standard KFM feedback loop.

[a]Electronic mail: robin@ifh.ee.ethz.ch
[b]Also with: Nanotechnology Group, Institute of Robotics, ETH Center/CLA, CH-8092 Zürich, Switzerland.
[c]Now with: Department of Chemistry, Harvard University, Cambridge, MA 02138.

 © 2000 American Institute of Physics

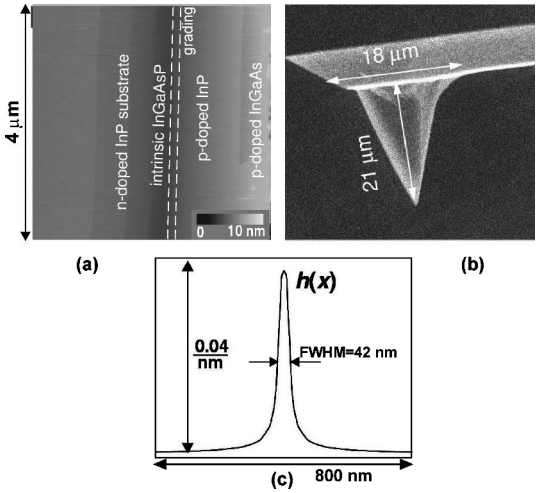

FIG. 2. (a) AFM picture (4 μm$\times$4 μm) of the topography of the $p-i-n$ laser structure, (b) SEM picture of the KFM tip, and (c) transfer function of the KFM tip.

raphy picture of the cleaved surface of the $p-i-n$ diode. This laser structure was particularly suited to our study as its constituting materials show low oxidation rates when exposed to the ambient air.[13]

First we have performed a KFM scan of the surface. The measured potential distribution is shown in Fig. 3. The potential difference between the n- and p-doped regions of the diode due to the equating Fermi levels is clearly visible on this figure. Figure 3(a) also shows the potential profile along the cutline $A-A'$ perpendicular to the structure. The potential drop between the n- and p-doped regions is measured to be equal to 600 mV which is substantially lower than the theoretical built-in voltage of a $p-n$ junction with the same doping levels which can be calculated to reach 1.3 V. The electric field distribution along cutline $A-A'$, shown in Fig. 3(b), was calculated by taking the first derivative of the potential profile. The spikes in the electric field allow us to very precisely locate the interfaces between the various layers. The spacing between the two central spikes yield an intrinsic InGaAsP layer thickness of 220 ± 20 nm. This value is 25% lower than the nominal value of 300 nm. The difference can be attributed to the fact that the $p-i-n$ laser was fabricated from a piece laying at the edge of the wafer where the layer

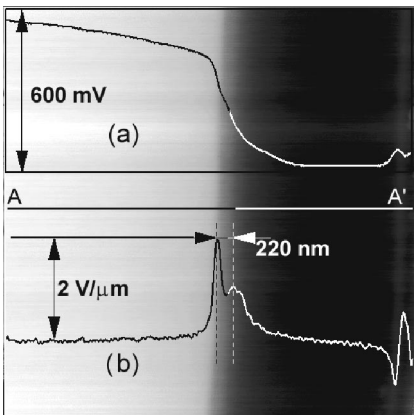

FIG. 3. Measured KFM potential of the InP/InGaAsP/InP $p-i-n$ laser structure and (a) potential and (b) electric field profiles along cutline $A-A'$. The scan area was 4 μm$\times$4 μm.

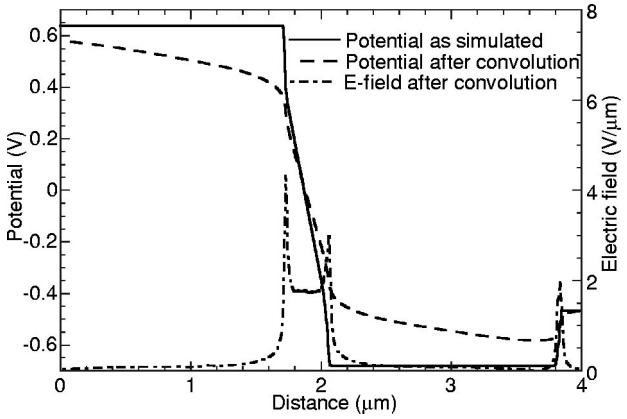

FIG. 4. One-dimensional cross-section of the two-dimensional simulated potential before (solid line) and after (dashed line) convolution with the tip transfer function and electric field (dashed-dotted line).

thicknesses depart from the nominal values as was confirmed by surface profiling measurements. The use of the grading at the interface p-InP/InGaAsP explains the lower and broader electric field spike compared to the the spike associated with the n-InP/InGaAsP interface.

Next, we performed simulations of the laser structure using the commercially available package ATLAS/BLAZE from SILVACO, Santa Clara, CA. The structure was simulated using a two-dimensional finite element grid structure. Great care was taken to match this structure to the measured one. We used an energy-balance model taking the nonlocal phenomena into account to describe carrier transport. A mobility model for electrons and holes given by Eq. (1) was employed which yields negative differential mobility for intermediate electric fields and a constant v_{sat} velocity for high electric fields:

$$\mu=\frac{\mu_0+\dfrac{v_{\mathrm{sat}}}{\mathcal{E}}\left(\dfrac{\mathcal{E}}{\mathcal{E}_{\mathrm{crit}}}\right)^{\gamma}}{1+\left(\dfrac{\mathcal{E}}{\mathcal{E}_{\mathrm{crit}}}\right)^{\gamma}}, \tag{1}$$

where $\mathcal{E}$ is the internal electric field, $\mathcal{E}_{\mathrm{crit}}$ is the electric field at which peak velocity occurs, μ_0 is the low-field mobility, and v_{sat} is the saturation velocity. For InP, given electron and hole effective masses of $m_e^*=0.078m_e$ and $m_h^*=0.603m_e$, respectively, the conduction- and valence-band densities of states N_C and N_V are calculated to be equal to 5.47×10^{17} and $1.15\times10^{19}\,\mathrm{cm}^{-3}$, respectively. Therefore, the doping level of the n-doped InP layer N_D being greater than N_C, this layer is found to be degenerated and Fermi–Dirac statistics was used instead of the approximated Boltzmann statistics. Figure 4 (solid line) shows a one-dimensional 1(D) cross-section of the two-dimensional simulated potential along a cutline perpendicular to the layers before convolution with the KFM tip-transfer function. The simulated potential difference between n- and p-doped regions is 1.31 V. Figure 4 (dashed line) also shows the simulated potential profile after convolution with the transfer function of the tip. Measured [Fig. 3(a)] and simulated (Fig. 4) potential are qualitatively very similar. The grading at the interface

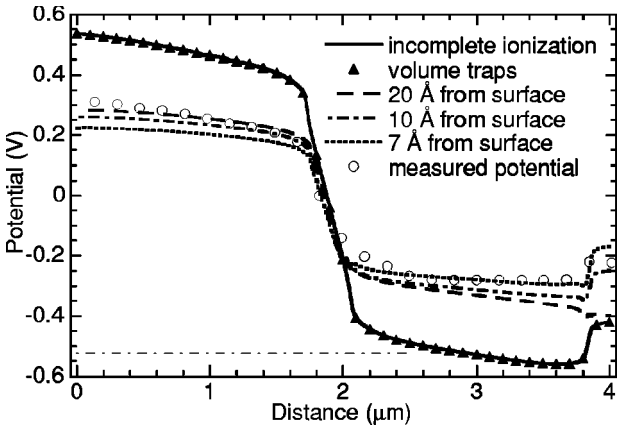

FIG. 5. Simulated potential after convolution with the tip transfer function: no traps (full line), volume traps (triangles), and interface traps at 2.0 nm from the surface (dashed line), 1.0 nm from the surface (dashed-dotted line), and 0.7 nm from the surface (dotted line). Comparison with KFM measurements.

InGaAsP/p-InP also induces a broadening of the simulated electric field spike (Fig. 4) in agreement with the KFM measurements.

Despite good qualitative agreement between measured and simulated potential profiles, the measured potential is seen to be approximately a factor 0.4 of the simulated one. To explain this discrepancy, we used additional models for our 2D simulations. Incomplete ionization of the donor atoms in the n-doped InP layer due to its degenerated nature was shown to take place by using a corresponding model[14] given by Eq. (2):

$$N_D^+ = \frac{N_D}{1 + g_D \exp\left(\dfrac{E_{F_n} - E_D}{kT}\right)}, \tag{2}$$

where g_D is the degeneracy factor for the conduction band and E_{F_n} is the quasi-Fermi level for electrons, decreasing the voltage difference by less than 0.1 V; this is not enough to explain the discrepancy with the KFM measurements. It is well-known that, despite the choice of materials with low oxidation rates, KFM measurements performed in the air lead to the adsorption of contaminants such as water and the creation of a native oxide or hydroxide $In(OH)_3$ which influence the work function of the materials under study. We accounted for such surface effects by implementing interface traps at the interface semiconductor air as well as volume traps in all layers of the structure (data taken from Iliadis *et al.*[15]). The surface charge was assumed to be uniform and independent of the materials and doping concentration. Figure 5 shows the simulated potential extracted at various distances from the surface after convolution with the KFM tip transfer function. The potential measured far away from the surface (influence of volume traps only) does not deviate significantly from the potential simulated without traps. However, Fig. 5 shows the influence of the fixed charges present at the interface semiconductor air on the reduction of the built-in potential of the $p-i-n$ junction as the potential profile is taken closer to the surface. Our simulator allowed us to obtain profiles as close at 0.7 nm. The simulated potential profile was fitted to the measured KFM potential and using a fixed charges surface concentration of $3 \times 10^{12}\,\mathrm{cm}^{-2}$ an excellent agreement was obtained.

In conclusion, we have measured a cross-sectional $p-i-n$ laser diode built-in potential profile and electric field with Kelvin probe force microscopy. 2D simulations show that the reduced potential drop compared to the theoretical value could be explained partly in terms of incomplete ionization of the donors in the degenerated n-doped region and partly by surface states. Combined use of KFM and 2D simulations offers new vistas for the characterization of semiconductor devices.

The authors wish to gratefully thank M. Kwakernaak for supplying the laser structure studied in this work.

[1] Y. Martin, D. W. Abraham, and H. K. Wickramasinghe, Appl. Phys. Lett. **52**, 1103 (1988).
[2] J. M. R. Weaver and D. W. Abraham, J. Vac. Sci. Technol. B **9**, 1559 (1991).
[3] M. Nonnenmacher, M. P. O'Boyle, and H. K. Wickramasinghe, Appl. Phys. Lett. **58**, 2921 (1991).
[4] A. Kikukawa, S. Hosaka, and R. Imura, Appl. Phys. Lett. **66**, 3510 (1995).
[5] H. O. Jacobs, P. Leuchtmann, O. J. Homan, and A. Stemmer, J. Appl. Phys. **84**, 1168 (1998).
[6] T. Mizutani, M. Arakawa, and S. Kishimoto, IEEE Electron Device Lett. **18**, 423 (1997).
[7] A. Chavez-Pirson, O. Vatel, M. Tanimoto, H. Ando, H. Iwamura, and H. Kanbe, Appl. Phys. Lett. **67**, 3069 (1995).
[8] C. M. Snowden, *Traditional Modeling of Semiconductor Devices*, in NATO ASI series. Series B, Physics (Plenum, New York 1995), Vol. 342, pp. 41–76.
[9] T. Suemitsu, T. Enoki, N. Sano, M. Tomizawa, and Y. Ishii, IEEE Trans. Electron Devices **45**, 2390 (1998).
[10] H. O. Jacobs, H. F. Knapp, S. Müller, and A. Stemmer, Ultramicroscopy **69**, 39 (1997).
[11] H. O. Jacobs, H. F. Knapp, and A. Stemmer, Rev. Sci. Instrum. **70**, 1756 (1999).
[12] H. O. Jacobs and A. Stemmer, Surf. Interface Anal. **27**, 361 (1999).
[13] M. Fukuda, IEEE J. Quantum Electron. **19**, 1692 (1983).
[14] R. C. Jaeger and F. H. Gaensslen, IEEE Trans. Electron Devices **27**, 914 (1980).
[15] A. A. Iliadis, S. C. Laih, and E. A. Martin, Appl. Phys. Lett. **54**, 1436 (1989).